Journal of Catalysis **190,** 75–91 (2000)
doi:10.1006/jcat.1999.2738, available online at http://www.idealibrary.com on IDEAL®

Infrared Study of NO Adsorption and Reduction with C_3H_6 in the Presence of O_2 over CuO/Al_2O_3

Yawu Chi and Steven S. C. Chuang[1]

Department of Chemical Engineering, The University of Akron, Akron, Ohio 44325-3906

Received June 4, 1999; revised October 19, 1999; accepted October 19, 1999

NO, NO/O_2, NO_2, and NO_2/O_2 adsorption on CuO/Al_2O_3 and selective catalytic reduction (SCR) of NO by C_3H_6 in the presence of 2% O_2 were investigated by infrared spectroscopy coupled with mass spectroscopy to provide insight into the mechanism of NO adsorption and reduction. Adsorption studies show that NO/O_2 adsorption at 298–723 K led to rapid formation of $Cu^{2+}<^{O}_{O}>N$ and gradual formation of adsorbed $(NO_3^-)_2$; NO_2/O_2 adsorption led to immediate formation of $(NO_3^-)_2$ and gradual formation of $^{Cu^{2+}-O}_{Cu^{2+}-O}>N$–O, $Cu^{2+}<^{O}_{O}>N$–O, and $Cu^{2+}<^{O}_{O}>N$; NO_2 adsorption alone did not produce $(NO_3^-)_2$. Temperature-programmed desorption shows that adsorbed $(NO_3^-)_2$ decomposed to N_2, N_2O, and NO at 644 K. Pulsing C_3H_6 into NO/O_2 over CuO/Al_2O_3 not only removed $(NO_3^-)_2$ but also reduced Cu^{2+} to Cu^+/Cu^0, resulting in the formation of N_2, N_2O, CO_2, and H_2O. Steady-state $NO/O_2/C_3H_6$ reaction on CuO/Al_2O_3 produced adsorbed C_3H_7–NO_2, CH_3COO^-, Cu^+–NCO, Cu^0–CN, and Cu^+–CO species, and N_2, CO_2, and H_2O as products. Dynamic behavior of adsorbates under transient conditions suggests that the steady-state SCR reaction may proceed via adsorbed C_3H_7–NO_2, Cu^0–CN, and Cu^+–NCO intermediates on Cu^0/Cu^+ surfaces. This study demonstrates that the pulse and steady-state SCR follows different reaction pathways toward N_2 and CO_2 products. © 2000 Academic Press

Key Words: **NO adsorption; nitrate formation; NO/O_2 adsorption; selective catalytic reduction; CuO/Al_2O_3; reaction mechanism; reaction intermediates; infrared spectroscopy; adsorbed nitrate.**

INTRODUCTION

The development of an effective catalyst for NO decomposition and reduction in an oxidizing environment has been one of the most challenging tasks in environmental catalysis (1–21). Voluminous work has been done on catalyst screening and characterization to unravel the detrimental effect of oxygen in the NO decomposition to N_2 and O_2 (3–10). Addition of a reducing agent is required for the selective conversion of NO to N_2 in the presence of O_2 (3–5, 7, 8, 12–18).

[1] To whom correspondence should be addressed. E-mail: schuang@uakron.edu. Fax: (330) 972-5856.

CuO/Al_2O_3 was selected in the present study as a model catalyst for the NO adsorption and reduction studies for the following reasons: (i) the Cu surface state has been well characterized by examination of the infrared spectra of adsorbed CO and NO (22–25); (ii) Cu-exchanged ZSM-5 has been shown to be the most active NO decomposition catalyst; and (iii) Cu/Al_2O_3 has exhibited activity for NO reduction with CO and NH_3 (26, 27). Since the selective catalytic reduction (SCR) of NO_x is a redox reaction, a fundamental understanding of the Cu oxidation states and their adsorbates holds the key to the development of a NO decomposition and reduction mechanism and the determination of the limitation of CuO/Al_2O_3 for these reactions.

The objective of this study is to determine the structure and dynamic behavior of adsorbates as well as the oxidation states of adsorption sites for NO adsorption and reduction with C_3H_6 in the presence of O_2 over CuO/Al_2O_3. Infrared spectroscopy (IR) coupled with mass spectroscopy (MS) is used to determine the sequence of adsorbate and product formation for elucidation of reaction pathways and the nature of sites. The adsorbates observed in this study include $^{Cu^{2+}-O}_{Cu^{2+}-O}>N$–O, $Cu^{2+}<^{O}_{O}>N$–O, $Cu^{2+}<^{O}_{O}>N$, and $Cu^{2+}(NO_3^-)_2$ during the NO/O_2 adsorption as well as R–NO_2 (R = alkyl group), CH_3COO^-, Cu^+–NCO, Cu^0–CN, and Cu^+–CO species during the steady-state $NO/O_2/C_3H_6$ reaction. It has been reported that the SCR with hydrocarbons and/or NH_3 produced $^{Cu^{2+}-O}_{Cu^{2+}-O}>N$–O, $Cu^{2+}<^{O}_{O}>N$–O, $Cu^{2+}<^{O}_{O}>N$, and $Cu^{2+}(NO_3^-)_2$ on Cu/Al_2O_3 (13, 27, 29); R–NO_2 and/or R–ONO on $Cu–Cr/Al_2O_3$ (29), Pt/SiO_2 and Ce–ZSM-5 (3, 30, 31), Co–ZSM-5 (5, 32), Cu–ZSM-5 (33), and Na–H–mordenite (34); CH_3COO^- on Pt/Al_2O_3 (35) and Al_2O_3 (36); isocyanate (–NCO) on Cu/Al_2O_3 (28, 37), $Cu–Cs/Al_2O_3$ (38), Cu–ZSM-5 (13), Rh–Al–MCM-41 (39), and Pt/Al_2O_3 (35); and cyanide (–CN) species on Cu/Al_2O_3 (28), Pt/Al_2O_3 (35), Cu/ZrO_2 (40), and Co–ZSM-5 (41). The knowledge of adsorbate reactivities and their dynamic behavior may serve as a basis for the development of a comprehensive mechanism for the SCR of NO_x with hydrocarbons.

0021-9517/00 $35.00

EXPERIMENTAL

Catalyst Precursor Preparation and Infrared (IR) Characterization

Copper nitrate/γ-Al_2O_3 was prepared by impregnation of γ-Al_2O_3 (Alfa Products, SA = 100 m^2/g, pore size = 0.01–0.02 μm) with $Cu(NO_3)_2 \cdot 3H_2O$ (Strem Chemicals) solution. The sample, denoted as $Cu(NO_3)_2 \cdot H_2O/Al_2O_3$, was dried overnight in air at 298 K. The Cu loading on the catalyst was 2.7 wt%. The amount of water was not determined. To obtain high resolution of infrared spectra for $Cu(NO_3)_2$, both $Cu(NO_3)_2 \cdot H_2O/Al_2O_3$ and $Cu(NO_3)_2 \cdot 3H_2O$ were mixed with KBr (Alfa Products, KBr spectrograde, ultrapure) at a KBr/catalyst weight ratio of 10 : 1, and then were pressed into self-supporting disks for infrared characterization at 298 K. $Cu(NO_3)_2 \cdot H_2O/Al_2O_3$, which was not mixed with KBr, was further characterized by IR spectroscopy coupled with temperature-programmed decomposition (TPDE) at a heating rate of 10 K/min from 298 to 773 K in a 75 cm^3/min He flow. The surface state of CuO/Al_2O_3 before and after NO/O_2 adsorption and SCR was characterized by IR spectroscopy with pulse CO chemisorption at 298 K.

Temperature-Programmed Desorption (TPD) of NO_x Adsorbates over CuO/Al_2O_3

The CuO/Al_2O_3 produced from temperature-programmed decomposition of $Cu(NO_3)_2 \cdot H_2O/Al_2O_3$ was used as the catalyst in this study. The CuO/Al_2O_3 was pretreated in a He flow at 773 K for 1 h and cooled to the desired temperature prior to each experiment. NO_x (i.e., NO, NO_2, and NO_3^-) adsorbates on CuO/Al_2O_3 were produced by flowing various NO_x reactant gas mixtures (0.08% NO + 2% O_2 + 97.92% He; 1.06% NO_2 + 98.94% He; 0.08% NO_2 + 2% O_2 + 97.92% He) at 298, 523, 623, and 723 K. Gases used were 1.01% NO with He balance (AGA Specialty Gas), 99.99% O_2 (Praxair), 99.999% He (Praxair), C_3H_6 (LINDE Specialty Gas), and 99.994% CO (Praxair). Infrared analysis found less than 0.02% N_2O in the certified 1.01% NO. TPD of NO_x adsorbates on CuO/Al_2O_3 was performed from the adsorbing temperature (298 and 523 K) to 773 K at a heating rate of 10 K/min in a 75 cm^3/min He flow.

Pulsing C_3H_6 into the Steady-State NO/O_2 Flow and Steady-State SCR Reaction of $NO/O_2/C_3H_6$ over CuO/Al_2O_3

Upon both adsorbate and reactant/product concentrations reaching the steady state during a constant NO/O_2 flow, selective catalytic reduction (SCR) of NO was carried out by pulsing 1 cm^3 of C_3H_6 into the steady-state flow of NO and O_2 at 0.1 MPa and 523, 623, and 723 K. Three consecutive pulses of 1 cm^3 of C_3H_6 were used in the SCR of NO to increase the NO conversion. Steady-state SCR reaction of 0.08% NO + 2% O_2 + 0.2% C_3H_6 + 97.72% He on CuO/Al_2O_3 was also conducted at a total flow rate of 75 cm^3/min, 0.1 MPa, and 523, 623, 673, 698, 723, and 773 K. The O_2-to-NO ratio of 25 used in this study is in the lower region of the exhaust composition for lean burn combustion engines and power plants.

Infrared Spectroscopy, Mass Spectrometer, and X-Ray Diffraction (XRD) Analyses

Variation in adsorbate concentration was determined by using a Nicolet 5SCX FTIR spectrometer at 4 cm^{-1} resolution. Infrared spectra were obtained by 32 coadded scans, which take 4 s for completion. Each coadded spectrum collected during TPD represents the average spectra of adsorbates during 1 K increases in temperature. Coadding a large number of scans increases the signal-to-noise ratio, but requires a longer sampling time, resulting in the loss of transient information. Hence, 32 coadded scans were used in the present study. Variation in reactant/product concentration was determined by using a Balzers QMG 112 and a Prisma QMS 200 mass spectrometer (MS) (Pfeiffer Vacuum Technology). The mass-to-charge ratios (m/e, i.e., amu) for MS monitoring were $m/e = 4$ for He, $m/e = 28$ for N_2 and CO, $m/e = 12$ (CO fragment) for separation of CO from $m/e = 28$, $m/e = 30$ for NO, $m/e = 32$ for O_2, $m/e = 44$ for N_2O and CO_2, $m/e = 22$ (CO_2 double ionization) for separation of CO_2 from $m/e = 44$, $m/e = 46$ for NO_2, and $m/e = 41$ for C_3H_6. The contribution of N_2O and NO_2 to $m/e = 30$ was determined by comparing the relative intensities of the fragment and parent ions of the calibrated N_2O, NO, and NO_2 pulse responses; the contribution of CO_2 to $m/e = 28$ was found to be negligible. The MS profiles of the reactants and products were obtained by multiplying their MS intensities by their calibration factors (42). The crystalline phases of CuO/Al_2O_3 were determined by using a Philips Analytical X-ray diffractometer with Cu $K\alpha$ radiation.

RESULTS

IR Spectra of $Cu(NO_3)_2 \cdot H_2O/Al_2O_3$ and $Cu(NO_3)_2 \cdot 3H_2O$

Figure 1 compares the IR spectra of $Cu(NO_3)_2 \cdot H_2O/Al_2O_3$ and $Cu(NO_3)_2 \cdot 3H_2O$ at 298 K. The IR spectrum of $Cu(NO_3)_2 \cdot H_2O/Al_2O_3$ was obtained by subtracting the Al_2O_3/KBr spectrum from the $Cu(NO_3)_2 \cdot H_2O/Al_2O_3$/KBr spectrum; the IR spectrum of $Cu(NO_3)_2 \cdot 3H_2O$ was obtained by subtracting the KBr spectrum from the $Cu(NO_3)_2 \cdot H_2O$/KBr spectrum. KBr has high IR transmission as shown in the inset. Bands below 1200 cm^{-1} for $Cu(NO_3)_2 \cdot H_2O/Al_2O_3$ were blocked by the Al_2O_3 support. Bands in the 1616–1636 cm^{-1} and 3400–3500 cm^{-1} regions are due to H_2O. $Cu(NO_3)_2 \cdot 3H_2O$ exhibited bands at 1767, 1385, and 823 cm^{-1} which is consistent with those reported

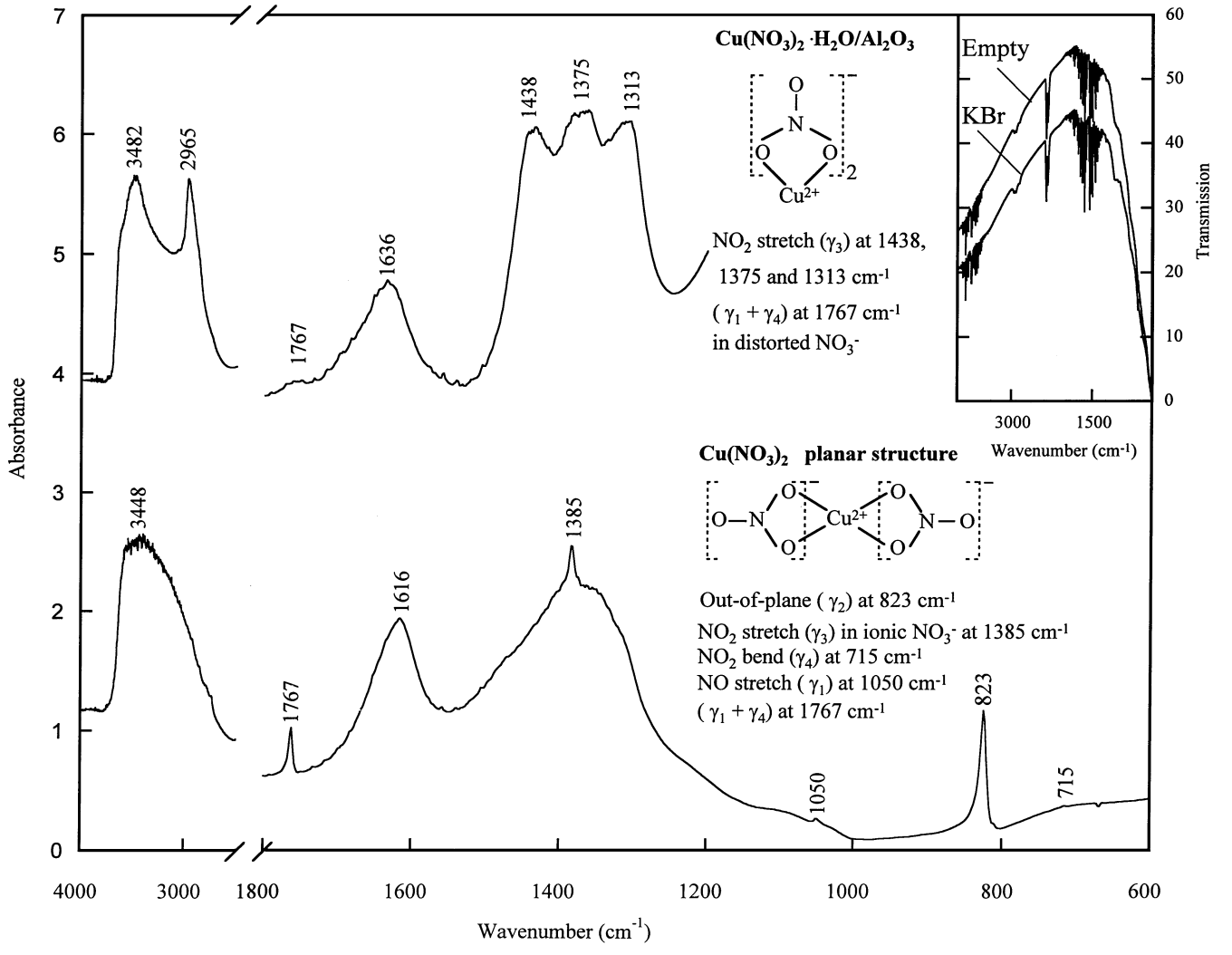

FIG. 1. IR spectra of $Cu(NO_3)_2 \cdot H_2O/Al_2O_3$ and $Cu(NO_3)_2 \cdot 3H_2O$ (infrared spectra of pure KBr as background and empty cell were inserted) at 298 K.

for $Cu(NO_3)_2$ (43–45). The band assignment is shown in Fig. 1. $Cu(NO_3)_2 \cdot H_2O$ on Al_2O_3 exhibited a strong triplet in the 1313–1438 cm^{-1} region, which may be due to the distortion from the D_{3h} of a NO_3^- species to the C_{2v} of a coordinated nitrato–ONO_2 species (43–45).

Temperature-Programmed Decomposition (TPDE) of $Cu(NO_3)_2 \cdot H_2O/Al_2O_3$

Figure 2 shows the normalized MS intensity product profiles and *in situ* IR spectra taken during the temperature-programmed decomposition (TPDE) of $Cu(NO_3)_2 \cdot H_2O/Al_2O_3$. Absorbance spectra of $Cu(NO_3)_2 \cdot H_2O/Al_2O_3$ during TPDE were obtained by ratioing the transmission spectra of $Cu(NO_3)_2 \cdot H_2O/Al_2O_3$ to that of CuO/Al_2O_3 at the specific temperature. CuO/Al_2O_3 transmission spectra, which were reserved as background spectra, were collected while the reactor cooled from 773 to 298 K in a He flow after TPDE. $Cu(NO_3)_2 \cdot H_2O$ exhibited a broad band in the 1305–1442 cm^{-1} region, in contrast to the clear triplet bands observed for $Cu(NO_3)_2 \cdot H_2O/Al_2O_3$ mixed with KBr in Fig. 1. Dilution of $Cu(NO_3)_2 \cdot H_2O/Al_2O_3$ with KBr in Fig. 1 increased the resolution of the triplet bands due to distorted $[NO_3^-]_2$. To avoid the complication from NO adsorption on KBr, $Cu(NO_3)_2 \cdot H_2O/Al_2O_3$ and CuO/Al_2O_3 resulting from $Cu(NO_3)_2 \cdot H_2O/Al_2O_3$ TPDE were not mixed with KBr during TPD and reaction studies. $Cu(NO_3)_2 \cdot H_2O/Al_2O_3$ began to decompose at 360 K, releasing H_2O, NO, N_2O, N_2, O_2, and NO_2. The MS intensity profiles were normalized with the calibration factors of each species so that the shaded area under the MS profiles corresponded to the product amount in micromoles. Evolution of adsorbed H_2O corresponds to the gradual decrease of the water band at 1620–1667 cm^{-1}. The peak temperature for the H_2O MS profile at 465 K is lower than those for NO, N_2O, and N_2 (at 485 K). The formation of these gaseous

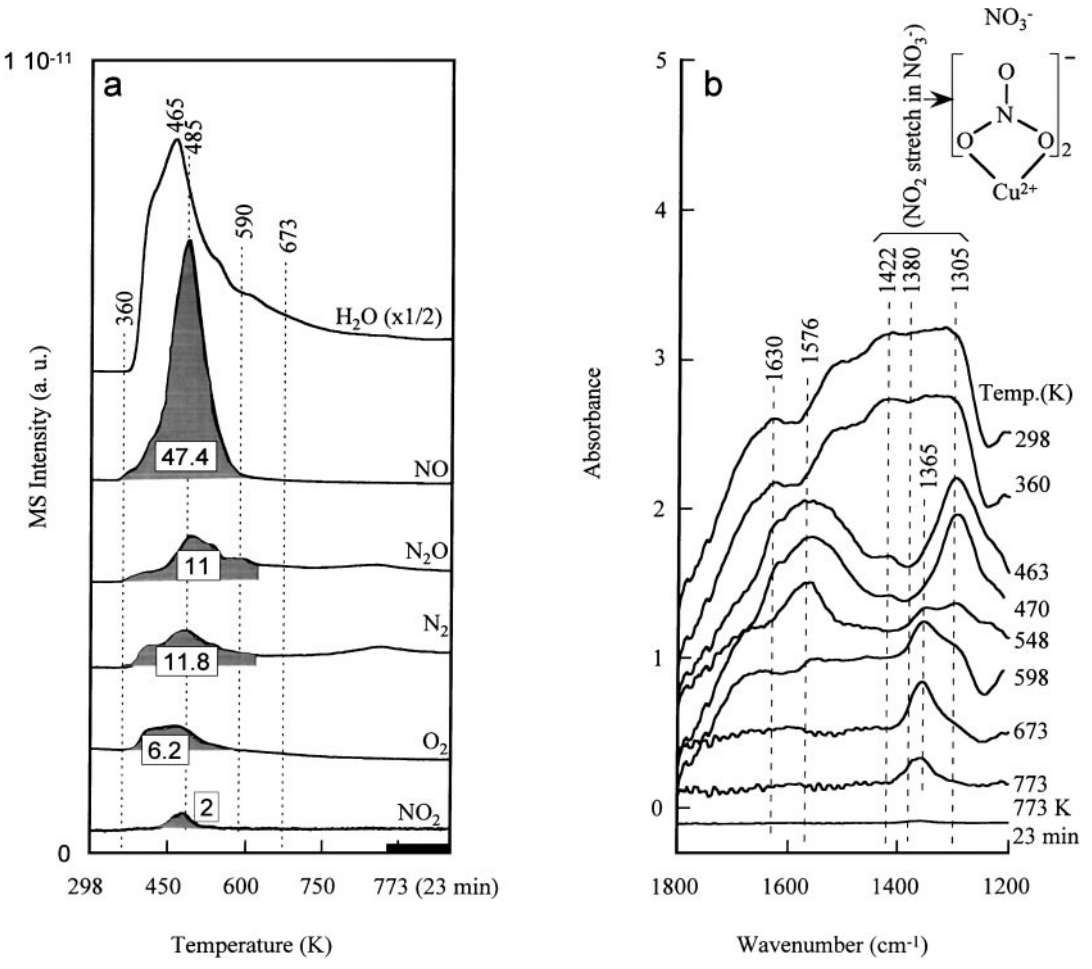

FIG. 2. (a) Normalized product MS profiles and (b) *in situ* IR spectra taken during the $Cu(NO_3)_2 \cdot H_2O/Al_2O_3$ decomposition from 298 to 773 K at a heating rate of 10 K/min. (H_2O MS profile was decreased by multiplying by $\frac{1}{2}$.)

species corresponding to a significant drop in the distorted $[NO_3^-]_2$ intensity indicates the decomposition of $Cu(NO_3)_2$ on Al_2O_3 to NO, N_2O, N_2, O_2, and NO_2. The amount of decomposed product is indicated in micromoles in Fig. 2a, giving a N/O ratio of 1.3 and a NO/O_2 ratio of 7.8. It is indeed surprising to observe the formation of a significant amount of N_2 and O_2. Increasing the temperature to 673 K produced a well-defined band at 1365 cm^{-1} with a shift to 1370 cm^{-1} at 773 K.

No direct information is available to distinguish the difference between the species giving broad bands at 1422, 1380, and 1305 cm^{-1} and the adsorbed species giving the single band at 1365–1370 cm^{-1}. We tentatively assign the singly symmetric band at 1365–1380 cm^{-1} to $(NO_3^-)_2$ since it resembles in some aspects that of $Cu^{2+}(NO_3^-)_2$. The appearance of this feature at temperatures above 548 K suggests that it is formed from the decomposition product of $Cu(NO_3)_2 \cdot H_2O/Al_2O_3$. To distinguish the difference between the singly symmetric band at 1365–1390 cm^{-1} and the broad triplet bands in the same region, we denote the former as $(NO_3^-)_2$, the undistorted structure, and the latter as $[NO_3^-]_2$, the distorted structure.

X-ray diffraction analysis (XRD) of the decomposed $Cu(NO_3)_2 \cdot H_2O/Al_2O_3$ gave only the γ-Al_2O_3 pattern (not shown). No XRD pattern for CuO or CuO_x was observed, suggesting that $Cu(NO_3)_2 \cdot H_2O/Al_2O_3$ decomposed to highly dispersed Cu oxide (46). The decomposed $Cu(NO_3)_2 \cdot H_2O/Al_2O_3$, denoted as CuO/Al_2O_3, was used as a catalyst for the NO decomposition and reduction studies. Further characterization of the CuO/Al_2O_3 surface state by IR studies of CO adsorption will be presented and discussed later.

TPD of Adsorbates on CuO/Al_2O_3 from 298/523 to 773 K

Figure 3 shows the normalized product MS intensity profiles and *in situ* IR spectra of adsorbed NO_x species on CuO/Al_2O_3 taken during TPD from 298 to 773 K. Figure 3b shows that exposure of CuO/Al_2O_3 to a 0.08% NO + 2% O_2 + 97.92% He flow at 298 K produced bands

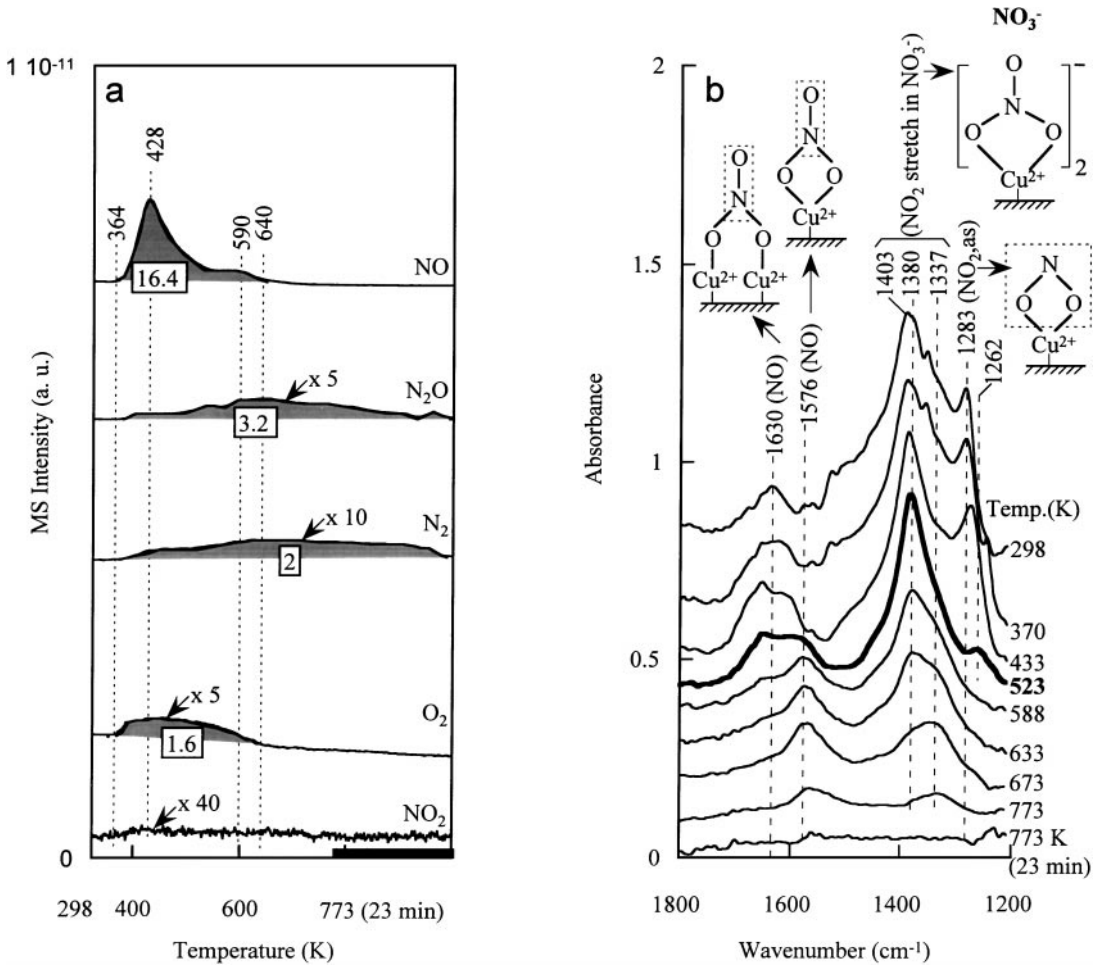

FIG. 3. (a) Normalized product MS profiles and (b) *in situ* IR spectra taken during the TPD of adsorbates (produced from flow of 0.08% NO + 2% O_2 + 97.92% He at 298 K) over CuO/Al_2O_3 from 298 to 773 K at a heating rate of 10 K/min. (N_2O, N_2, O_2, and NO_2 MS profiles were enlarged by multiplying by 5, 10, 5, and 40, respectively.)

at 1403, 1380, and 1337 cm^{-1}, bridging bidentate nitrate ($^{Cu^{2+}-O}_{Cu^{2+}-O}$>N–O) at 1630 cm^{-1}, chelating bidentate nitrate ($Cu^{2+}<^{O}_{O}$>N–O) at 1576 cm^{-1}, and the overlapping component of their NO_2 asymmetric vibration with chelating nitro ($Cu^{2+}<^{O}_{O}$>N) at 1283 cm^{-1} (15, 16, 47–52). These adsorbates may be associated with Cu^{2+} sites as observed in the CO adsorption studies discussed in the latter part of this study, which showed that the CuO/Al_2O_3 exposed to NO/O_2 contained Cu^{2+} sites. It should be noted that the notation used for these adsorbed NO_x species did not include the charge balance. The charge on Cu^{2+} is expected to be balanced by the surface oxygen anion and adsorbed nitrate/nitro species. The bands at 1403, 1380, and 1337 cm^{-1} resembled those observed on $Cu(NO_3)_2 \cdot H_2O/Al_2O_3$, and can be assigned to the NO_2 stretch of a distorted $[NO_3^-]_2$ adsorbed on Cu^{2+}.

The distorted $[NO_3^-]_2$ adsorbed on CuO/Al_2O_3 began decomposing at 364 K, releasing NO, N_2O, N_2, and O_2 (Fig. 3). The amount (micromoles) of products released, equivalent to the area under the product profile, is also indicated Fig. 3a. Evolution of NO and O_2, the primary products in the 364–640 K region, corresponds to the gradual decrease in the IR intensities of $^{Cu^{2+}-O}_{Cu^{2+}-O}$>N–O at 1630 cm^{-1}, $[NO_3^-]_2$ at 1380 cm^{-1}, and $Cu^{2+}<^{O}_{O}$>N at 1262–1278 cm^{-1}. Increasing the temperature to 523 K caused the broad distorted $[NO_3^-]_2$ band to sharpen. Increasing the temperature to 588 K produced $Cu^{2+}<^{O}_{O}$> N–O at 1576 cm^{-1}. $Cu^{2+}<^{O}_{O}$>N–O, also observed during $Cu(NO_3)_2/Al_2O_3$ decomposition in the 463–548 K region in Fig. 2b, could be produced from the readsorption of NO and O_2. In fact, NO/O_2 adsorption on CuO/Al_2O_3 at 523 K confirmed the formation of dominant $Cu^{2+}<^{O}_{O}$> N–O. A further increase in temperature from 588 to 773 K caused the $(NO_3^-)_2$ to shift from 1380 to 1337 cm^{-1}. Evolution of N_2O and a small fraction of N_2 at temperatures above 673 K corresponded to decreases in the IR intensities of both $Cu^{2+}<^{O}_{O}$>N–O at 1576 cm^{-1} and $[NO_3^-]_2$ at 1337 cm^{-1}. Comparison of the MS profiles in Fig. 3a with those in Fig. 2a shows that NO and O_2 desorption exhibited similar profiles. The major difference is that N_2O and N_2

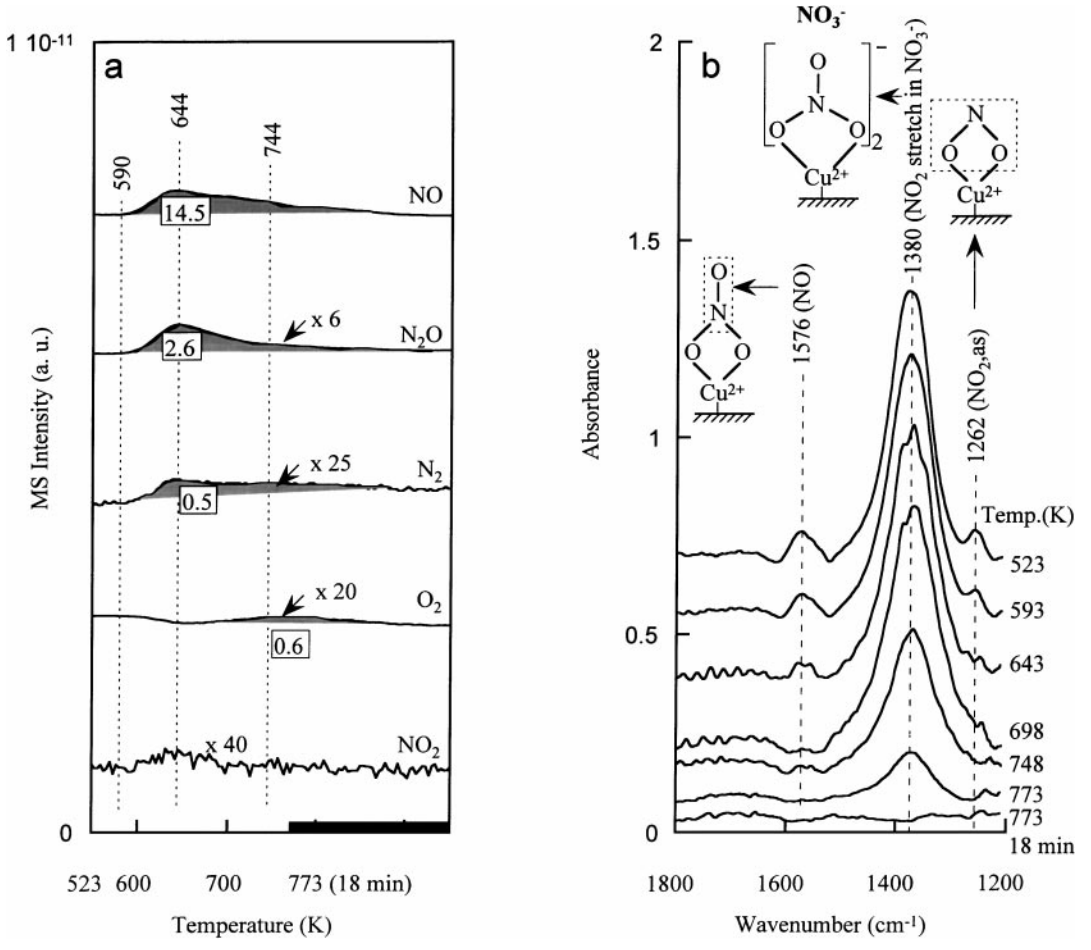

FIG. 4. (a) Normalized product MS profiles and (b) *in situ* IR spectra taken during the TPD of adsorbates (produced from flow of 0.08% NO + 2% O_2 + 97.92% He at 523 K) over CuO/Al_2O_3 from 523 to 773 K at a heating rate of 10 K/min. (N_2O, N_2, O_2, and NO_2 MS profiles were enlarged by multiplying by 6, 25, 20, and 40, respectively.)

profiles lagged behind those of NO and O_2 with the presence of $Cu^{2+}<^{O}_{O}>N–O$ in the 588–773 K region in Fig. 3a.

Figure 4 shows the normalized product MS intensity profiles and *in situ* IR spectra of adsorbed NO_x species on CuO/Al_2O_3 taken during TPD from 523 to 773 K. Adsorbed $(NO_3^-)_2$ at 1380 cm^{-1}, $Cu^{2+}<^{O}_{O}>N–O$ at 1576 cm^{-1}, and $Cu^{2+}<^{O}_{O}>N$ at 1262 cm^{-1} produced from NO/O_2 adsorption at 523 K began to decompose at 590 K, releasing NO, N_2O, and N_2 with peak intensities at 644 K. Comparison of product MS profiles and IR spectra of adsorbates in Fig. 4 to those in Fig. 3 suggests that desorption/decomposition of distorted $[NO_3^-]_2$, $^{Cu^{2+}–O}_{Cu^{2+}–O}>N–O$, and $Cu^{2+}<^{O}_{O}>N$ were responsible for O_2 and part of the NO formation at 428 K, while $(NO_3^-)_2$ at 1380 cm^{-1} and $Cu^{2+}<^{O}_{O}>N–O$ were mainly responsible for the NO, N_2O, and N_2 formation at around 644 K.

Adsorption of NO and O_2 on CuO/Al_2O_3

Figure 5 shows *in situ* IR spectra produced from the coadsorption of 0.08% NO and 2% O_2 at 298, 523, and 623 K as well as 0.08% NO adsorption followed by 2% O_2 at 523 K on CuO/Al_2O_3. Flowing 0.08% NO/2% O_2 over CuO/Al_2O_3 at 298 K produced the chelating nitro $Cu^{2+}<^{O}_{O}>N$ at 1262 cm^{-1}, $^{Cu^{2+}–O}_{Cu^{2+}–O}>N–O$ at 1620 cm^{-1}, and adsorbed $NO^{\delta-}$ at 1836 cm^{-1}. Prolonged exposure to NO/O_2 produced $Cu^{2+}<^{O}_{O}>N–O$ at 1576 and 1283 cm^{-1} and the $(NO_3^-)_2$ band at 1380 cm^{-1} in addition to nitro and bridging bidentate nitrate (15, 16, 47–52). Flowing 0.08% NO/2% O_2 at 523 K produced the same adsorbates as those produced at 298 K, but at a higher formation rate than that at 298 K. The overlapping of $Cu^{2+}<^{O}_{O}>N$ at 1251 cm^{-1} with $Cu^{2+}<^{O}_{O}>N–O$ at 1262 cm^{-1} results in the formation of a prominent band at 1262 cm^{-1}. The significant fraction of 1262 cm^{-1} is due to the NO_2 asymmetric vibration of $Cu^{2+}<^{O}_{O}>N$ rather than that of $Cu^{2+}<^{O}_{O}>N–O$ since $Cu^{2+}<^{O}_{O}>N–O$ gives a lower intensity at 1262 cm^{-1} than at 1570 cm^{-1}. The amount of adsorbed NO determined by the NO MS profile (not shown) is 0.50 mol per mole of Cu^{2+} at 523 K.

Exposure of CuO/Al_2O_3 to 0.08% NO at 523 K produced $Cu^{2+}<^{O}_{O}>N–O$ at 1570 and 1233 cm^{-1}, nitrito (Cu^{2+}–O–N=O) at 1315 cm^{-1}, and chelating nitro $Cu^{2+}<^{O}_{O}>N$ at

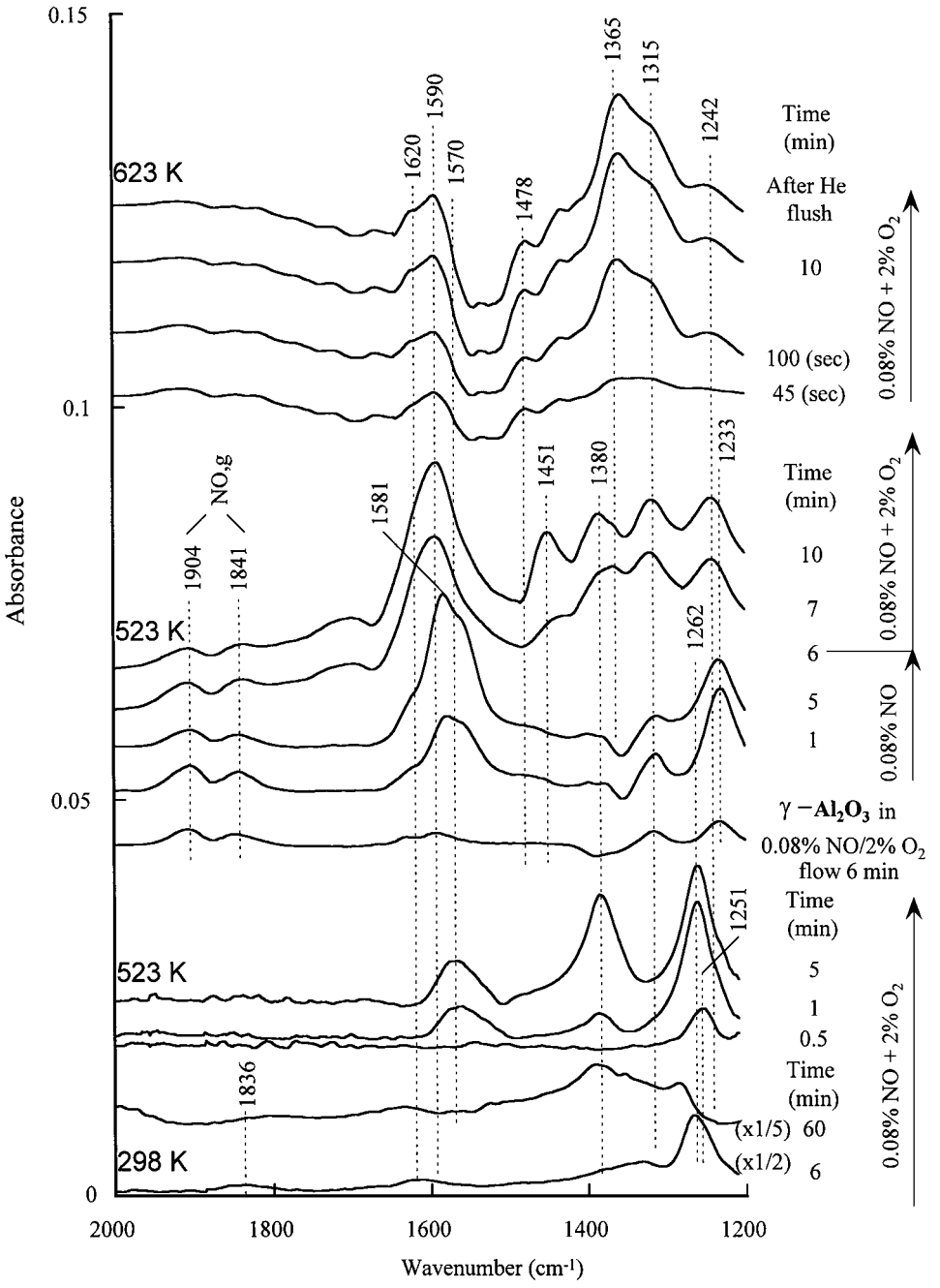

FIG. 5. *In situ* IR spectra produced from (a) flow of 0.08% NO + 2% O_2 + 97.92% He at 523 K, (b) flow of 0.08% NO followed by 2% O_2 addition at 523 K, and (c) flow of 0.08% NO + 2% O_2 + 97.92% He at 623 K over CuO/Al_2O_3.

1233 cm^{-1}. Addition of 2% O_2 to a 0.08% NO flow at 523 K resulted in (i) the formation of monodentate nitrate Cu^{2+}–O–N$<^{O}_{O}$ at 1451 cm^{-1} and $(NO_3^-)_2$ at 1380 cm^{-1} and (ii) the shift in wavenumber of $Cu^{2+}<^{O}_{O}>$N–O from 1570 to 1590 cm^{-1} and that of $Cu^{2+}<^{O}_{O}>$N from 1233 to 1242 cm^{-1}. Formation of $(NO_3^-)_2$ and Cu^{2+}–O–N$<^{O}_{O}$ and an increase in the intensity of $Cu^{2+}<^{O}_{O}>$N–O after O_2 addition suggests the successive oxidation of $Cu^{2+}<^{O}_{O}>$N and Cu^{2+}–O–N=O to the various forms of adsorbed nitrates.

The most interesting feature for 0.08% NO/2% O_2 coadsorption on CuO/Al_2O_3 at 623 K is the rapid formation of dominant $(NO_3^-)_2$ centered at 1365 cm^{-1}. High temperature is responsible for the low intensity of $Cu^{2+}<^{O}_{O}>$N as well as its wavenumber shift at 623 K. This is further confirmed by the absence of $Cu^{2+}<^{O}_{O}>$N for NO/O_2 coadsorption at 723 K. The absence of gaseous NO_2 formation over CuO/Al_2O_3 indicated that these adsorbed nitrates and nitro groups are formed from the reaction of NO and O_2 on

CuO without a gaseous NO_2 intermediate. The formation of $Cu^{2+}<^{O}_{O}>N$ and $Cu^{2+}<^{O}_{O}>N–O$ from NO/O_2 adsorption is thermodynamically favorable (53). The contribution of Al_2O_3 to adsorbate formation on CuO/Al_2O_3 was not significant as evidenced by low intensities of $Al^{3+}<^{O}_{O}>N$ at 1233 cm^{-1}, $Al^{3+}–O–N=O$ at 1315 cm^{-1}, $^{Al^{3+}-O}_{Al^{3+}-O}>N–O$ at 1630 cm^{-1}, and $Al^{3+}<^{O}_{O}>N–O$ at 1590 cm^{-1} in Fig. 5. The intensities of these adsorbates are less than 5% of those on CuO/Al_2O_3. Therefore, Cu sites are responsible for the formation of $Cu^{2+}(NO_3^-)_2$ from flowing 0.08% NO + 2% O_2 + 97.92% He over CuO/Al_2O_3.

Adsorption of NO_2/O_2, and NO_2 on CuO/Al_2O_3

Figure 6 compares the IR spectra of adsorbates produced from NO_2 and from NO_2/O_2 adsorption on CuO/Al_2O_3 at 523 K. Initial exposure of CuO/Al_2O_3 to 0.08% NO_2 + 2% O_2 + 97.92% He at 523 K produced $Cu^{2+}(NO_3^-)_2$ at 1380 cm^{-1} first, then $Cu^{2+}<^{O}_{O}>N–O$ at 1590 and 1561 cm^{-1}, $^{Cu^{2+}-O}_{Cu^{2+}-O}>N–O$ at 1620 cm^{-1}, and $Cu^{2+}<^{O}_{O}>N$ centered at 1262 cm^{-1}. NO_2 adsorption alone cannot produce $Cu^{2+}(NO_3^-)_2$ at 1380 cm^{-1}; however, it produced primarily $Cu^{2+}<^{O}_{O}>N–O$. The simultaneous presence of

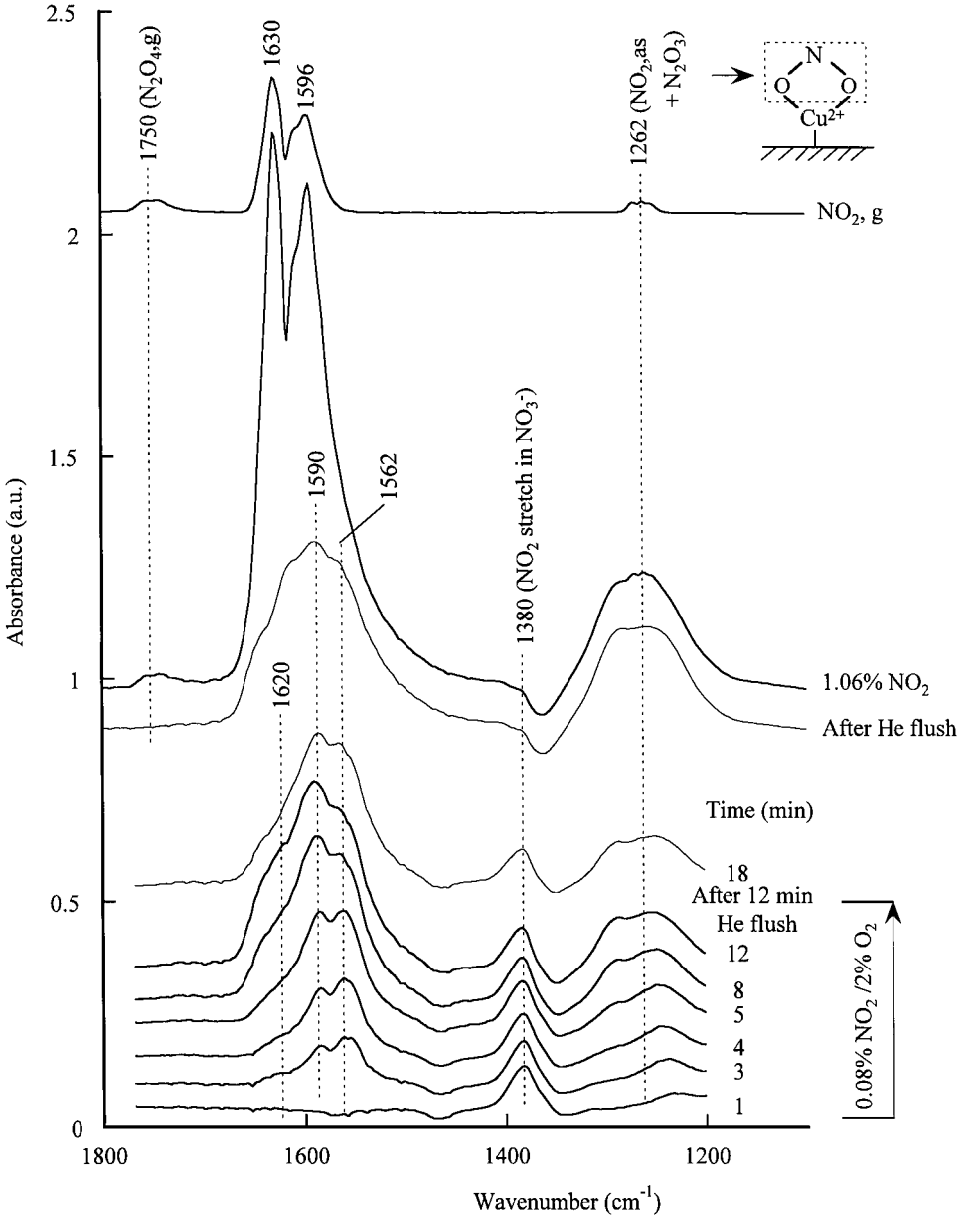

FIG. 6. *In situ* IR spectra of adsorbates produced from flow of 1.06% NO_2 and from flow of 0.08% NO_2 + 2% O_2 + 97.92% He over CuO/Al_2O_3 at 523 K for 12 min (thin solid lines were taken after He flush.)

O_2 and NO_2 is required to produce $Cu^{2+}(NO_3^-)_2$ at 1380 cm^{-1}. This observation suggested that O_2 is necessary for $Cu^{2+}(NO_3^-)_2$ formation. The IR intensity of the band at 1262 cm^{-1} for NO_2 as well as NO_2/O_2 adsorption was stronger than that for NO/O_2 adsorption. This band can be assigned to the overlap component of $Cu^{2+}<^{O}_{O}>N$ and adsorbed N_2O_3 (16). At 523 K, NO_2/O_2 adsorption produced a dominant $Cu^{2+}<^{O}_{O}>N–O$ band while the NO/O_2 adsorption produced an intense $Cu^{2+}(NO_3^-)_2$ band.

Pulsing C_3H_6 into Steady-State NO/O_2 Flow and Steady-State SCR Reaction of $NO/O_2/C_3H_6$ on CuO/Al_2O_3

Figure 7 shows the MS profiles and *in situ* IR spectra taken while three consecutive 1-cm^3 C_3H_6 pulses were pulsed into the steady-state 0.08% NO + 2% O_2 + 97.92% He flow at 723 K. Pulsing C_3H_6 decreased the NO and O_2 MS intensity (i.e., concentration) and increased the N_2, CO_2, N_2O, H_2O, and NO_2 concentration. The MS profile of C_3H_6 led those of N_2, CO_2, N_2O, H_2O, and NO_2, consistent with the Langmuir–Hinshelwood mechanism (i.e., reactant adsorption followed by surface reaction and product desorption). Pulsing C_3H_6 also decreased the IR intensity of adsorbed $Cu^{2+}(NO_3^-)_2$ at 1365 cm^{-1}, indicating that this species may be the active adsorbate responsible for product formation. Gaseous CO_2 at 2358 and 2312 cm^{-1} emerged as one of the products. Observation of =C–H and C–H bands around 3100–2900 cm^{-1} was attributed to the incomplete consumption of C_3H_6. The band at 1561 cm^{-1} was attributed to NO_2 asymmetric vibration in $C_3H_7–NO_2$ (30, 31, 33, 34, 54, 55). The IR intensity of adsorbed $Cu^{2+}(NO_3^-)_2$ reached the minimum at 65 s, when NO and O_2 approached the minimum concentration.

Figure 8a shows that exposure of CuO/Al_2O_3 to a 0.08% NO + 2% O_2 + 0.2% C_3H_6 + 97.72% He flow at 523 K produced an organic nitro compound ($C_3H_7–NO_2$) at 1593 and

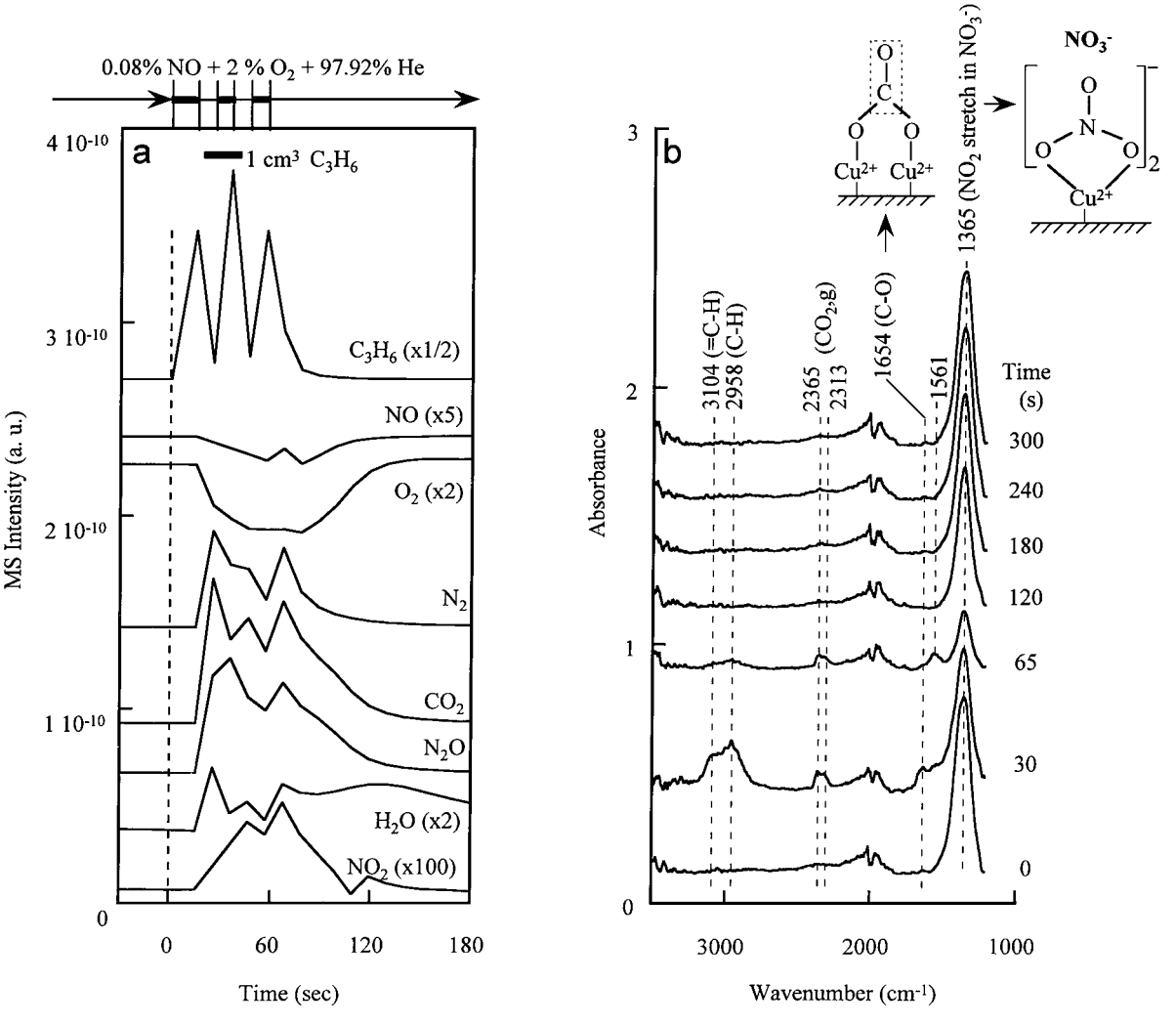

FIG. 7. (a) MS profiles and (b) *in situ* IR spectra taken during pulsing of three consecutive 1-cm^3 pulses of C_3H_6 into the steady-state flow of 0.08% NO + 2% O_2 + 97.92% He over CuO/Al_2O_3 at 723 K.

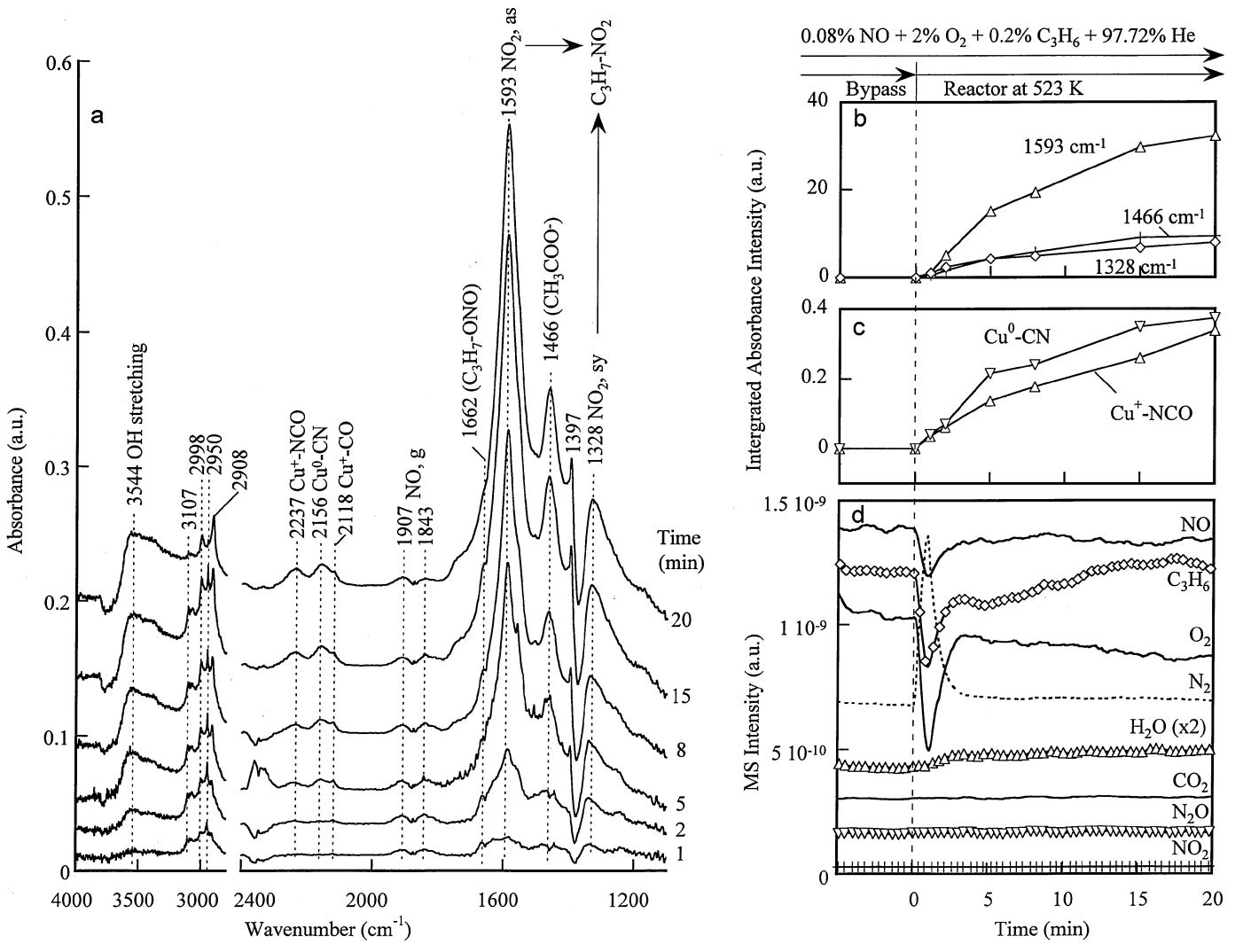

FIG. 8. (a) *In situ* IR spectra of adsorbates. (b) and (c) Integrated absorbance intensity as a function of time obtained from $\bar{A}_{1593} = \int_{1510}^{1780} A(\upsilon)\, d\upsilon$, $\bar{A}_{1466} = \int_{1410}^{1490} A(\upsilon)\, d\upsilon$, $\bar{A}_{1328} = \int_{1200}^{1370} A(\upsilon)\, d\upsilon$, $\bar{A}_{2156} = \int_{2124}^{2190} A(\upsilon)\, d\upsilon$, and $\bar{A}_{2237} = \int_{2200}^{2280} A(\upsilon)\, d\upsilon$, where A_i is the integrated absorbance intensity for species *i*. (d) MS profiles during switching the flow of 0.08% NO + 2% O_2 + 0.2% C_3H_6 + 97.72% He from bypass into the reactor at 523 K. (H_2O MS profile was enlarged by multiplying by 2.)

1328 cm^{-1} (30, 31, 33, 34, 54, 55), an organic nitrito compound (C_3H_7–ONO) at 1662 cm^{-1} (30, 31, 33, 34, 54, 55), an CH_3COO^- at 1593 and 1466 cm^{-1} (35, 36, 54–56), Cu^+–CO at 2118 cm^{-1} (25, 28), Cu^0–CN at 2156 cm^{-1} (28, 40, 41), Cu^+–NCO at 2237 cm^{-1} (28, 35, 57), the OH stretching band at around 3544 cm^{-1}, and C–H asymmetric stretching bands at 3107, 2998, 2950, and 2908 cm^{-1} (54, 55). The presence of gaseous NO indicated that NO was not reduced/oxidized completely. Absorbance intensity versus time profiles in Figs. 8b and 8c showed that initial formation rate of C_3H_7–NO_2 and CH_3COO^- was greater than that of Cu^0–CN and Cu^+–NCO. MS analysis of reaction products in Fig. 8d shows that initial exposure of CuO/Al_2O_3 to a $NO/O_2/C_3H_6$ flow caused a high overshoot in N_2 formation, corresponding to the decrease of NO, C_3H_6, and O_2 concentrations. The H_2O formation profile was enlarged by multiplying by 2 in Fig. 8d.

Table 1 gives the steady-state NO, C_3H_6, and O_2 conversion and N_2 selectivity results at different temperatures and reaction times. Increasing the temperature increased the NO, C_3H_6, and O_2 conversion. N_2 selectivity increased slightly with increasing temperature from 95% to 97%. Our Cu/Al_2O_3 shows activity similar to those reported but with a difference in N_2 yield (27–29).

Figure 9 shows the IR spectra taken during steady-state SCR reaction on Cu/Al_2O_3. Reaction conditions and selectivity results are listed in Table 1. Increasing the temperature caused the intensities of C_3H_7–NO_2, CH_3COO^-, and gaseous CO_2 to increase. To delineate the change in the contour of the IR bands in the 1350–1700 cm^{-1} region, the

TABLE 1

Reactant Conversion and N_2 Selectivity during Steady-State 0.08% NO + 6.67% O_2 + 0.2% C_3H_6 + 93.05% He Flow on CuO/Al_2O_3 at Various Temperatures

Temperature (K) and time on stream (min)	0.08% NO + 2% O_2 + 0.2% C_3H_6 + 97.72% He				
	Conversion (%)			Conversion of NO to N_2 (%)[a]	N_2 selectivity (%)[b]
	NO	C_3H_6	O_2		
523, 10	26.9	30.3	19.3	25.9	96.5
623, 15	35.7	35.0	21.6	34.2	95.7
673, 10	87.6	22.5	32.9	84.5	96.5
698, 10	90.4	29.4	33.8	88.0	97.4
723, 20	96.4	99.0	37.3	94.1	97.6
773, 25	100	100	39.1	97.3	97.3

[a] Conversion of NO to N_2 (%) = 2(mol N_2)/mol $NO_{in} \times 100$.
[b] N_2 selectivity (%) = 2(mol N_2)/(mol NO_{in} − mol NO_{out}) × 100.

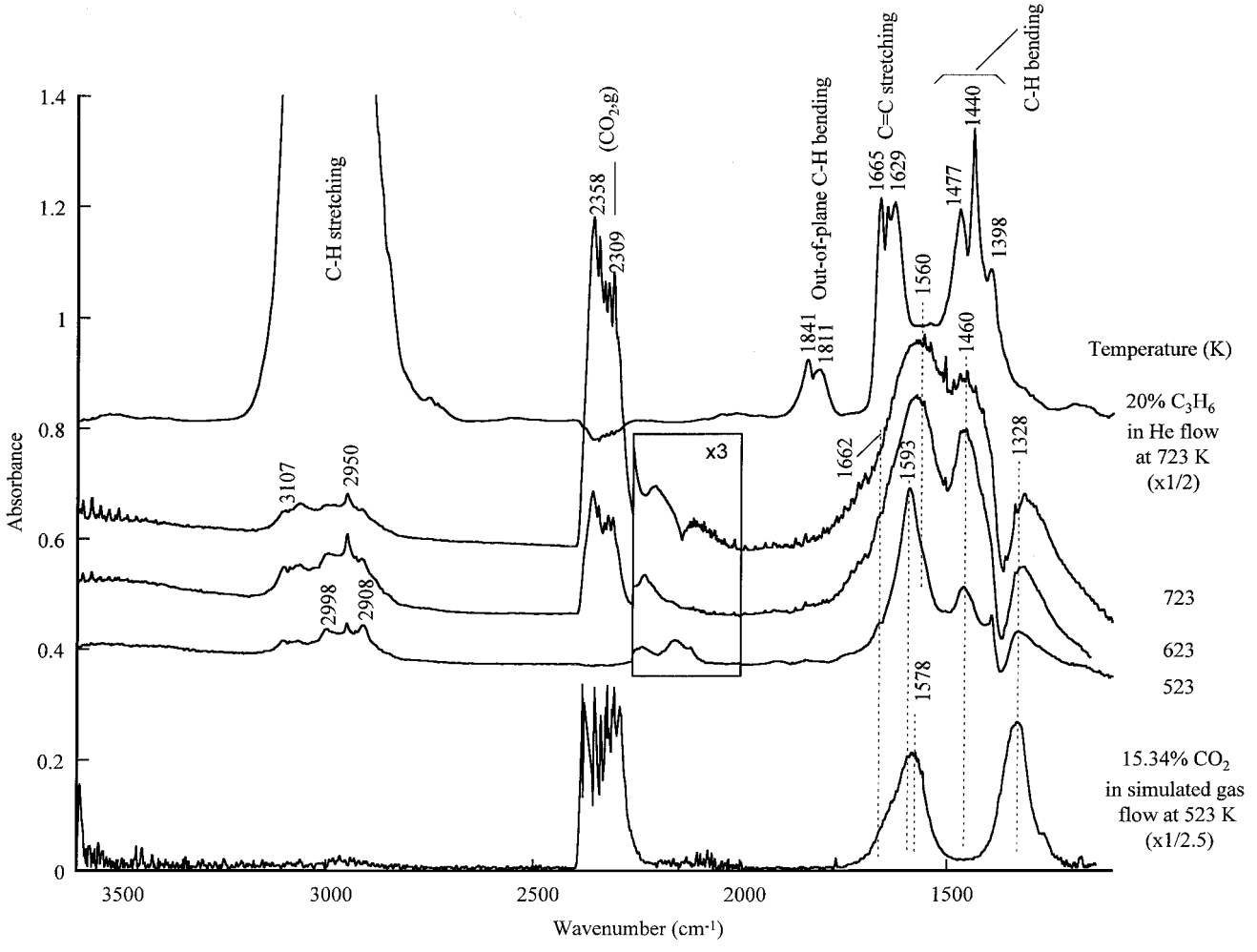

FIG. 9. Steady-state *in situ* IR spectra of adsorbates produced from flow of 0.08% NO + 2% O_2 + 0.2% C_3H_6 + 97.72% He over CuO/Al_2O_3 at various temperatures.

catalyst was exposed to C_3H_6 and automobile exhaust simulated gas (15.34% CO_2, 0.7765% CO, 0.5392% O_2, 0.2673% H_2, and 0.0865% C_3H_8 with He balance), respectively. Comparison of the IR spectra of adsorbates from C_3H_6 to that of $NO/O_2/C_3H_6$ adsorption on CuO/Al_2O_3 indicated that 1328, 1466, and 1593 cm^{-1} bands, attributed to C_3H_7–NO_2 and CH_3COO^-, cannot be formed from C_3H_6 adsorption alone. CO_2 adsorption from simulated gas on CuO/Al_2O_3 produced chelating carbonate ($Cu^{2+}<^{O}_{O}>C–O$) and monodentate carbonate ($Cu^{2+}–O–C<^{O}_{O}$) at 1578 and 1328 cm^{-1}, respectively (48). The ratio of IR intensity of the band at 1578 cm^{-1} to that of the band at 1328 cm^{-1} was 0.8 for carbonate; however, the ratio was 5.2 for $NO/O_2/C_3H_6$ reaction on CuO/Al_2O_3 at 523 K. The broadening of the 1593 and 1328 cm^{-1} bands at 623 and 723 K can be attributed to overlapping of carbonate bands with the C_3H_7–NO_2 and CH_3COO^- bands. The broadening of these bands is accompanied by strong gaseous CO_2 bands at 723 K, further confirming the contribution of carbonates from CO_2 adsorption.

The obvious effects of temperature are (i) the increase in the CH_3COO^- intensity at 1460 cm^{-1} and (ii) the shift in the wavenumber of the band from 1593 to 1560 cm^{-1}. To further unravel the dynamic behavior of C_3H_7–NO_2 at 1560 and 1314 cm^{-1} and of CH_3COO^- at 1460 cm^{-1}, the C_3H_6 flow was stopped while NO, O_2, and He flows were kept at steady state and 723 K. Figure 10 shows the variation of *in situ* IR spectra of adsorbates as a function of time after the C_3H_6 flow was stopped at 723 K. Disappearance of C_3H_6 resulted in (i) immediate disappearance of C_3H_6-related bands and (ii) a gradual decay of C_3H_7–NO_2 and CH_3COO^-. Upon disappearance of the C_3H_7–NO_2 and CH_3COOH species, gaseous NO_2 and adsorbed $Cu^{2+}(NO_3^-)_2$ emerged. The appearance of C_3H_7–NO_2 at 1560 cm^{-1} at 723 K is consistent with that of C_3H_7–NO_2 at 1561 cm^{-1} during the C_3H_6 pulse in Fig. 7b.

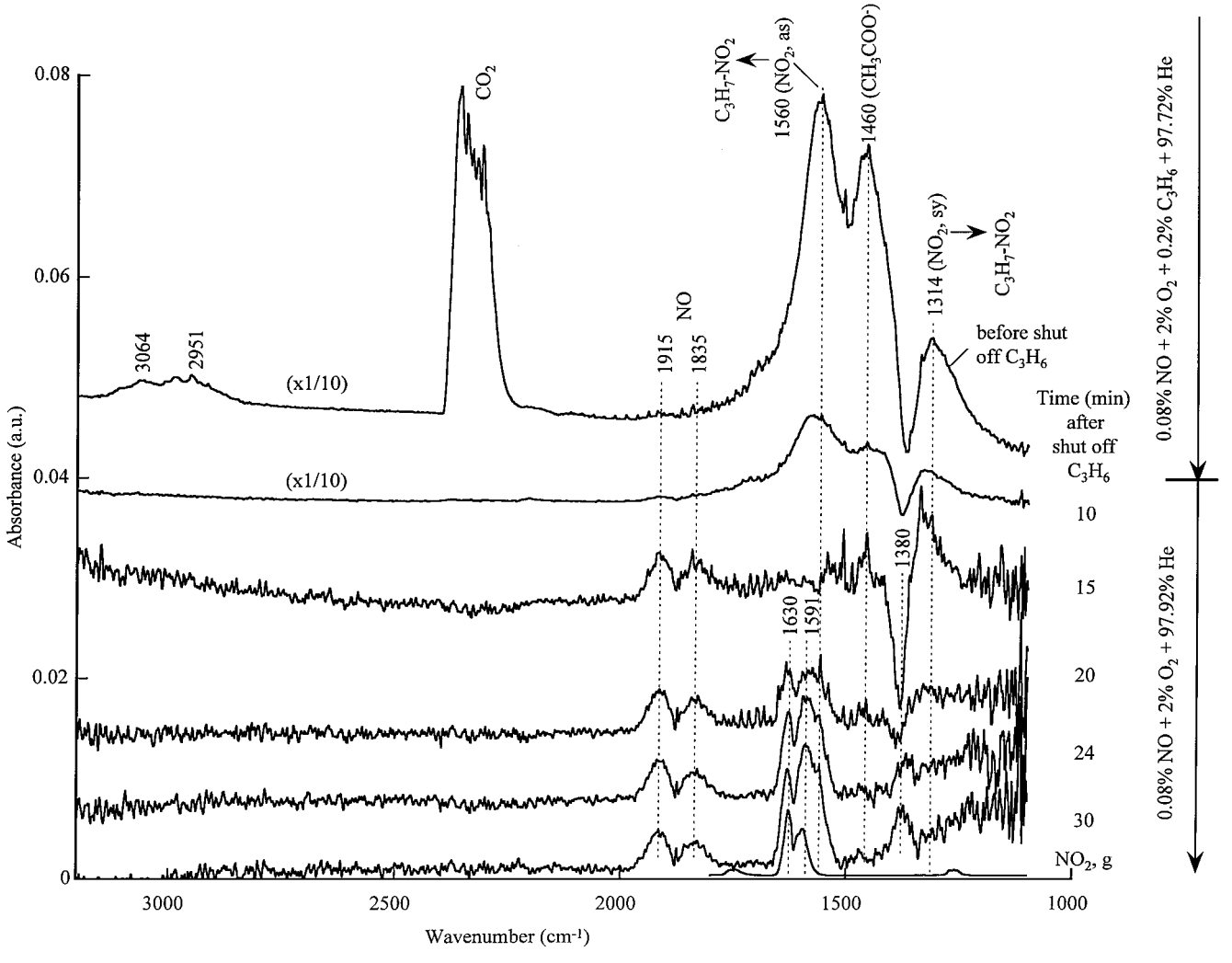

FIG. 10. Variation of *in situ* IR spectra of adsorbates as a function of time after shut-off of C_3H_6 from 0.08% NO + 2% O_2 + 0.2% C_3H_6 + 97.72% He flow over CuO/Al_2O_3 at 723 K.

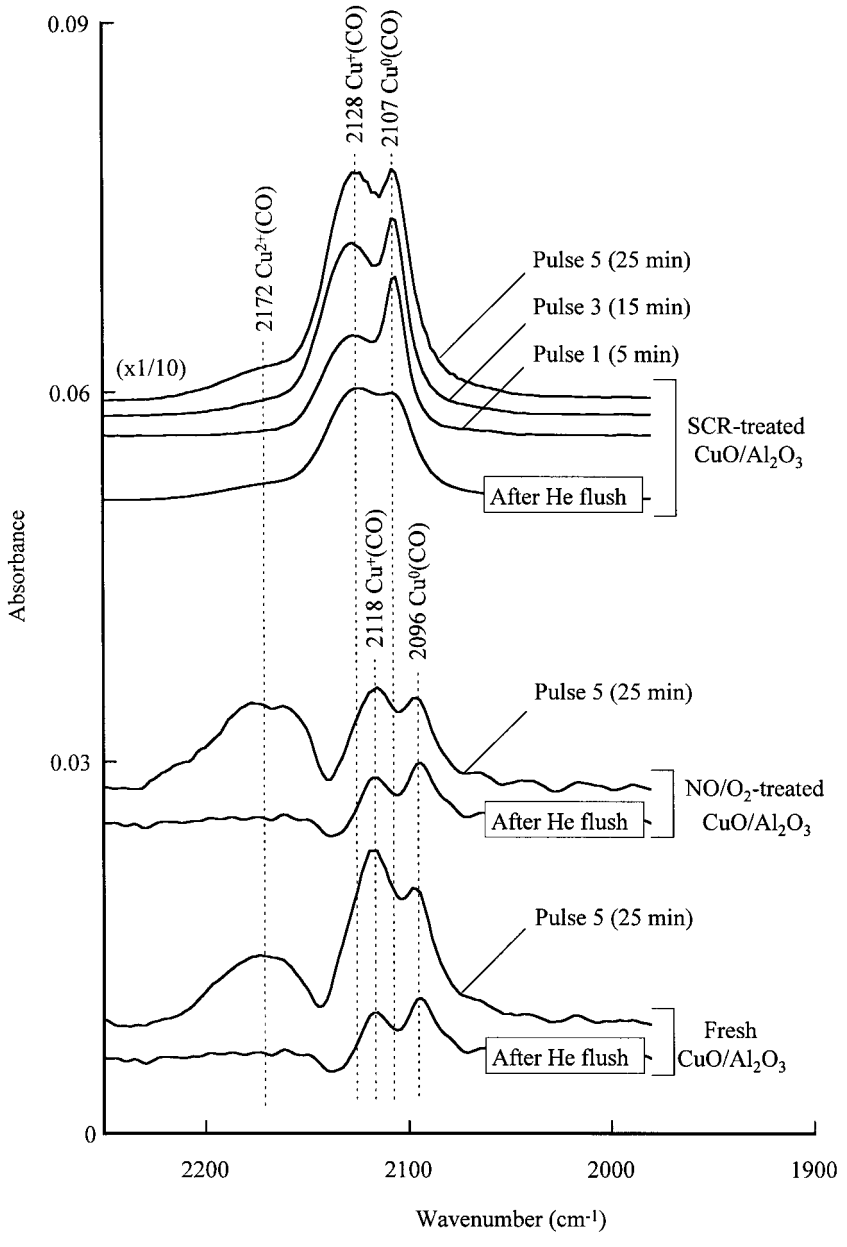

FIG. 11. *In situ* IR spectra taken during exposure of fresh CuO/Al_2O_3, NO/O_2-treated CuO/Al_2O_3, and SCR-treated CuO/Al_2O_3 to CO pulse (top spectrum for each catalyst) and after exposure to He flowing at 75 cm^3/min (bottom spectrum for each catalyst) for 5 min at 298 K. Fresh CuO/Al_2O_3 is produced from the thermal decomposition of $Cu(NO_3)$ on Al_2O_3 in He flow; NO/O_2-treated CuO/Al_2O_3 is obtained after NO/O_2, NO_2, NO_2/O_2 desorption and subsequent TPD studies; and SCR-treated CuO/Al_2O_3 is produced after SCR reaction at 773 K.

CO Chemisorption on CuO/Al_2O_3

Pulsing CO on fresh CuO/Al_2O_3 at 298 K produced $Cu^{2+}(CO)$ at 2172 cm^{-1} (25, 28, 37), $Cu^{+}(CO)$ at 2118 cm^{-1}, and $Cu^{0}(CO)$ at 2096 cm^{-1} (25), as shown in Fig. 11. Each CO pulse consists of 10 cm^3 of 99.994% CO. The IR spectra were collected immediately after the CO pulse. Pulsing CO allows the determination of the amount of CO adsorbed on the catalyst surface. CO preferably adsorbed on Cu^0 initially and then on Cu^+ over SCR-treated CuO/Al_2O_3. Flowing He over adsorbed CO species decreased the IR intensities of all species, consistent with the observations on Cu/Al_2O_3 at 300 K (25). No adsorbed CO was observed on γ-Al_2O_3 under the conditions of this study. Adsorption of CO on α-Al_2O_3 has been reported to give a band at 2150 cm^{-1} (58). The IR band intensity corresponds to the concentration of adsorbates, also reflecting the number of specific adsorption sites. However, the lack of extinction coefficients for

these various forms of adsorbed CO does not allow the use of these adsorbate intensities to determine the number of Cu^0, Cu^+, and Cu^{2+} sites. Qualitatively speaking, exposure of CuO/Al_2O_3 to the NO/O_2 flow decreased more Cu^+ than Cu^0 sites and converted a portion of Cu^0/Cu^+ sites to Cu^{2+} sites; the SCR reduced almost all Cu^{2+} sites to Cu^0/Cu^+ sites. Assuming the extinction coefficient for adsorbed CO is independent of its coverage, a significant increase in adsorbate intensity reflects the increase in the number of adsorption sites. The amount of CO adsorbed is determined to be 29.5 μmol for the SCR-treated catalyst and 2.5 μmol for the fresh CuO/Al_2O_3, indicating the SCR not only reduced Cu^{2+} to Cu^+/Cu^0 but also increased the dispersion of Cu^0/Cu^+ species on the Al_2O_3 surface.

DISCUSSION

Formation of Adsorbed NO_x from NO/O_2 and NO_2/O_2

The broad bands in the regions of 1500–1670 cm^{-1} and 1200–1350 cm^{-1} observed in this study result from overlapping of multiple bands. Although most of these bands cannot be unambiguously assigned, the observation of a singly symmetric band at 1380 cm^{-1} in Figs. 4, 6, and 7 as well as at 1242 cm^{-1} in Fig. 5 allows assignment of these bands to specific NO_x species. Band assignment here follows the classical works reported by Nakamoto (47) and Davydov (48), previous literature (21–45, 49–52), and the IR spectra of $Cu(NO_3)_2$ and $Cu(NO_3)_2 \cdot H_2O/Al_2O_3$ in Fig. 1.

Adsorption studies shown in Fig. 5 demonstrate that NO/O_2 adsorption on CuO/Al_2O_3 led to immediate formation of $Cu^{2+}{<}^{O}_{O}{>}N$ and gradual formation of $Cu^{2+}(NO_3^-)_2$ at 523 K; Fig. 6 shows that NO_2/O_2 adsorption led to immediate formation of $Cu^{2+}(NO_3^-)_2$ and gradual formation of $^{Cu^{2+}-O}_{Cu^{2+}-O}{>}N{-}O$, $Cu^{2+}{<}^{O}_{O}{>}N{-}O$, and $Cu^{2+}{<}^{O}_{O}{>}N$. NO_2 adsorption alone did not lead to the formation of $Cu^{2+}(NO_3^-)_2$; NO_2 adsorption produced only $^{Cu^{2+}-O}_{Cu^{2+}-O}{>}N{-}O$, $Cu^{2+}{<}^{O}_{O}{>}N{-}O$, and $Cu^{2+}{<}^{O}_{O}{>}N$ species. It is hoped that the adsorbate dynamics will provide insight into the reaction pathways during NO/O_2 adsorption and the SCR of NO_x in the presence of O_2.

Figure 12 illustrates the pathway for the formation of NO_x species. The thickness of the arrow indicates the rate of each step (e.g., thicker arrow for higher rate). The Cu site which is associated with $(NO_3^-)_2$ appears to be in the

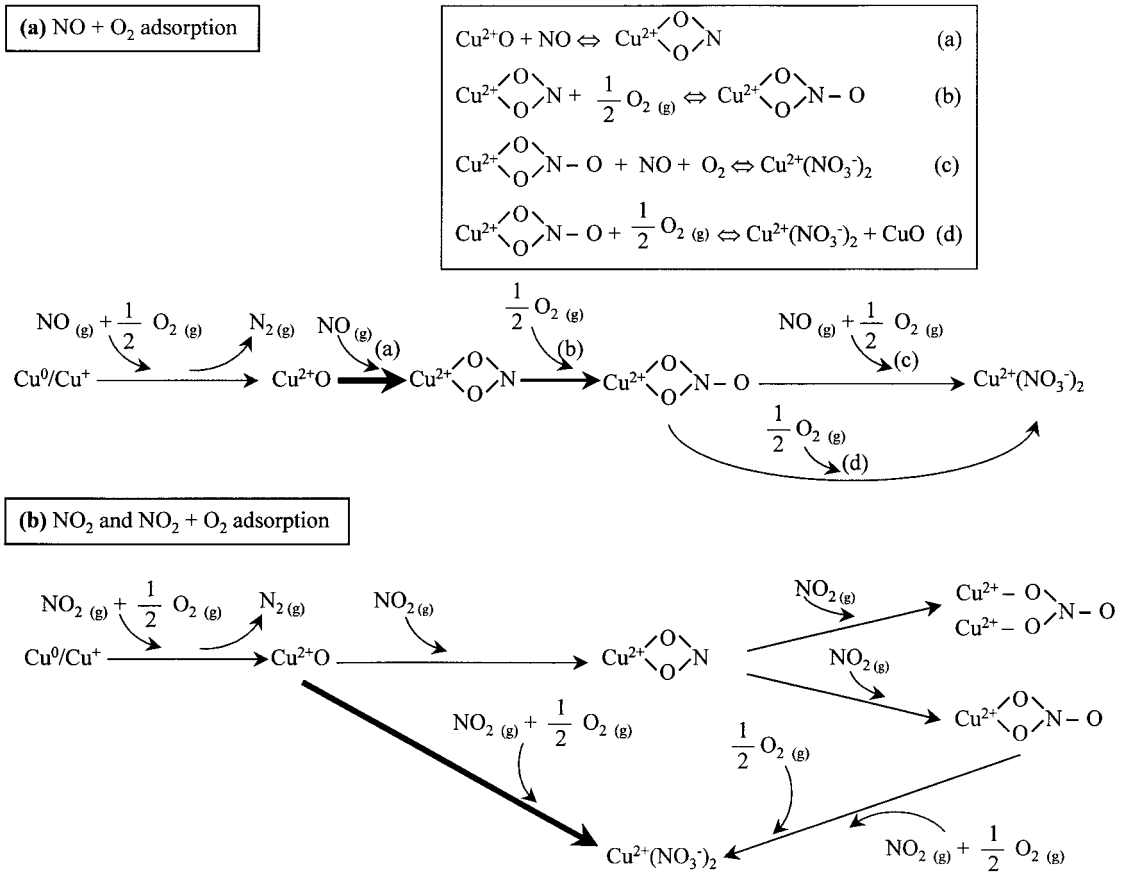

FIG. 12. Proposed pathway for (a) 0.08% NO + 2% O_2 adsorption and (b) 1.06% NO_2 and 0.08% NO_2 + 2% O_2 adsorption over CuO/Al_2O_3.

2+ state since (i) the IR spectrum of these adsorbed $(NO_3^-)_2$ species in Figs. 5 and 6 resembles that of $Cu^{2+}(NO_3^-)_2$ and (ii) NO/O_2 exposure not only produced $Cu^{2+}(NO_3^-)_2$ but also caused a significant increase in Cu^{2+} sites, as shown in Fig. 11.

Formation of $Cu^{2+}(NO_3^-)_2$ from NO/O_2 adsorption can be written as a series of well-defined steps, (a), (b), (c), and (d) in Fig. 12. Step (a) is evidenced by the formation of $Cu^{2+}<^{O}_{O}>N$ from NO adsorption on CuO/Al_2O_3 shown in Fig. 5. Step (b) describes the growth of $Cu^{2+}<^{O}_{O}>N–O$ upon addition of O_2. Steps (c) and (d) are supported by the observation of (i) rapid growth of $Cu^{2+}(NO_3^-)_2$ at high temperature (i.e., 623 K) and (ii) conversion of $Cu^{2+}<^{O}_{O}>N–O$ to $Cu^{2+}(NO_3^-)_2$ upon increasing the temperature from 523 to 623 K (not shown) (59).

All of the steps involved in the formation of $Cu^{2+}<^{O}_{O}>N–O$ from NO/O_2, NO_2/O_2, and NO_2 are thermodynamically favorable with a large negative value of ΔG° at 773 K (53). The formation of these adsorbed NO_x species from NO/O_2 rather than from pure NO_2 appears to be related to the nature of the site for adsorption rather than the thermodynamic driving force. The absence of $Cu^+(NO)$ at temperatures greater than 523 K suggests that Cu^+ and possibly Cu^0 sites are oxidized to Cu^{2+} during the NO/O_2 and NO_2/O_2 adsorption processes.

SCR Pathway

IR results of pulsing C_3H_6 and steady-state SCR studies in Figs. 7–10 show that the catalyst surface states and their adsorbates are strongly influenced by reaction environment (i.e., partial pressures of reactants and reaction temperature). Figure 13a illustrates the reaction pathways for the pulse SCR on CuO/Al_2O_3 according to the observed adsorbates and products. The NO/O_2 steady-state flow simulates the exhaust composition of lean burn combustion in which NO and O_2 adsorption on Cu/Al_2O_3 produced $Cu^{2+}(NO_3^-)_2$. These nitrates adsorbed primarily on Cu^{2+}. Each mole of Cu^{2+} on Al_2O_3 adsorbed approximately 0.50 mol of NO at 523 K. Increasing the temperature from 298 to 723 K decreased the amount of NO adsorbed on Cu/Al_2O_3. Pulsing C_3H_6 not only removed $(NO_3^-)_2$ adsorbed on Cu^{2+} species but also led to reduction of Cu^{2+} to Cu^0/Cu^+ and CO_2 formation. CuO/Al_2O_3 not only serves as a good sorbent for NO/O_2 but also exhibits high selectivity

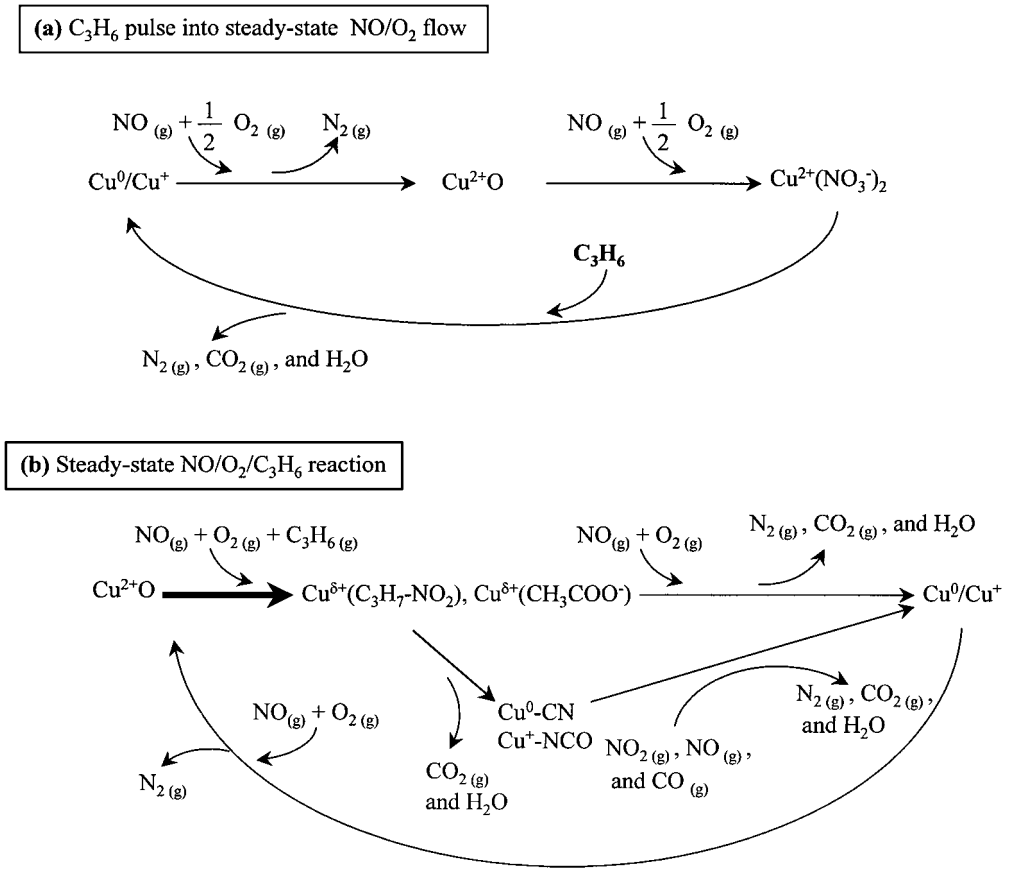

FIG. 13. Proposed pathway for (a) reaction between adsorbed $(NO_3^-)_2$ with C_3H_6 pulse and (b) steady-state SCR of NO with C_3H_6 in the presence of O_2 over CuO/Al_2O_3.

for converting $(NO_3^-)_2$ to N_2 with C_3H_6. Different forms of nitrates on Al_2O_3 (36) and Rh–Al–MCM-41 (39) have also been recently found to react with C_3H_6.

The key difference in adsorbates and Cu surface state between pulse and steady-state SCR can be simply attributed to the competitive adsorption of reactants. In the pulse SCR, NO/O_2 oxidizes the Cu in CuO/Al_2O_3 to Cu^{2+}, adsorbing $(NO_3)_2$ prior to the C_3H_6 pulse entering the reactor. In the steady-state SCR in Fig. 13b, C_3H_6 competes over NO/O_2 for adsorption, keeping Cu in either the Cu^0 or Cu^+ state and allowing the formation of C_3H_7–NO_2 and CH_3COO^-, as potential intermediates. These intermediates appear to be associated with either Cu^0/Cu^+ or Al_2O_3 surface sites since the catalyst contained fewer Cu^{2+} sites following the SCR as evidenced by the CO adsorption results in Fig. 11.

The proposed scheme in Fig. 13b suggests that adsorbed C_3H_7–NO_2 may be further converted to adsorbed Cu^0–CN and Cu^+–NCO species. The high initial rate of C_3H_7–NO_2 formation compared to that of Cu^0–CN formation in Figs. 8b and 8c further supports the conclusion that the reaction sequence proceeds via C_3H_7–NO_2 and then Cu^0–CN and Cu^+–NCO, since the proceeding intermediate has a higher initial rate than the subsequent intermediate in a consecutive reaction (60). The absence of C_3H_7–NO_2/CH_3COOH in the gas phase and the immediate disappearance of these species following termination of the C_3H_6 flow suggest that these species are unstable and may be reaction intermediates. No definite evidence is available to either support or dispute C_3H_5–NO_2/CH_3COO^- as active intermediates for the reaction. Although R–NO_2, R–ONO, and CH_3COO^- produced from the $NO/O_2/C_3H_6$ flow have been found to produce N_2 and CO_2 during their exposure to NO/O_2 (3, 30, 33, 34, 36, 61, 62), their role in the reaction mechanism needs to be further verified by using an isotopic tracing technique under reaction conditions where all the reactants and products are present.

CONCLUSIONS

Infrared spectroscopy coupled with mass spectroscopy allows the determination of the dynamic behavior of adsorbate and product formation during NO/O_2 adsorption, decomposition, and $NO/O_2/C_3H_6$ reaction. Adsorption studies from 298 to 723 K show that adsorption of NO/O_2, NO_2/O_2, and NO_2 produced various adsorbed nitrates on CuO/Al_2O_3. NO/O_2 adsorption led to immediate formation of $Cu^{2+}<^{O}_{O}>N$ and gradual formation of $Cu^{2+}(NO_3^-)_2$; NO_2/O_2 adsorption led to rapid formation of $Cu^{2+}(NO_3^-)_2$ and gradual formation of $^{Cu^{2+}-O}_{Cu^{2+}-O}>N$–O, $Cu^{2+}<^{O}_{O}>N$–O, and $Cu^{2+}<^{O}_{O}>N$; NO_2 adsorption produced only $^{Cu^{2+}-O}_{Cu^{2+}-O}>N$–O, $Cu^{2+}<^{O}_{O}>N$–O, and $Cu^{2+}<^{O}_{O}>N$ species. TPD studies show that adsorbed $(NO_3^-)_2$, the dominant nitrate, decomposed to N_2, N_2O, and NO at 644 K.

Steady-state $NO/O_2/C_3H_6$ reaction on CuO/Al_2O_3 produced adsorbed C_3H_7–NO_2, C_3H_5–ONO, CH_3COO^-, Cu^+–NCO, Cu^0–CN, and Cu^+–CO species, and N_2, CO_2, and H_2O as products. The dynamic behavior of adsorbates under transient conditions suggests that the steady-state SCR proceeds via adsorbed C_3H_7–NO_2, Cu^0–CN, and Cu^+–NCO intermediates on Cu^0/Cu^+ sites. Transient formation of N_2 from NO/O_2 adsorption on the fresh Cu/Al_2O_3 catalyst at 523 K was attributed to N–N bond formation on Cu^0 site from decomposed nitrate species. Production of N_2 is accompanied by the formation of a Cu^{2+} site, adsorbing NO and O_2 as $(NO_3^-)_2$. Pulsing C_3H_6 into NO/O_2 over $(NO_3^-)_2$ on the Cu^{2+} site not only reduced Cu^{2+} to Cu^+/Cu^0 but also converted $(NO_3^-)_2$ to N_2 and N_2O. Varying the reactant concentration changes the adsorbate concentration and shifts the reaction pathways for SCR.

ACKNOWLEDGMENTS

Although the research described in this article has been funded wholly by the United States Environmental Protection Agency under assistant agreement R823529-01-0 to the University of Akron, it has not been subject to the Agency's peer and administrative review and therefore may not necessarily reflect the views of the Agency, and no official endorsement should be inferred.

REFERENCES

1. Shelef, M., *Chem. Rev.* **95**, 209 (1995).
2. Iwamoto, M., *Catal. Today* **29**, 29 (1996).
3. Yokoyama, C., and Misono, M., *J. Catal.* **150**, 9 (1994).
4. Halasz, I., Brenner, A., Ng, K. Y. S., and Hou, Y., *J. Catal.* **161**, 359 (1996).
5. Sun, T., Fokema, M. D., and Ying, J. Y., *Catal. Today* **33**, 252 (1997).
6. Gervasini, A., *Appl. Catal. B* **14**, 147 (1997).
7. Kijlstra, W. S., Brands, D. S., Smit, H. I., Poels, E. K., and Bliek, A., *J. Catal.* **171**, 219 (1997).
8. Hwang, I. C., Kim, D. H., and Woo, S. I., *Catal. Today* **44**, 47 (1998).
9. Acke, F., and Skoglundh, M., *J. Phys. Chem. B* **97**, 972 (1999).
10. Burch, R., Fornasiero, P., and Watling, T. C., *J. Catal.* **176**, 204 (1998).
11. Valyon, J., and Hall, W. K., *J. Phys. Chem.* **97**, 1204 (1993).
12. Li, Y., and Armor, J. N., *Appl. Catal. B* **5**, L257 (1995).
13. Hoost, T. E., Laframboise, K. A., and Otto, K., *Appl. Catal. B* **7**, 79 (1995).
14. Bethke, K. A., Li, C., Kung, M. C., Yang, B., and Kung, H. H., *Catal. Lett.* **31**, 287 (1995).
15. Adelman, B. J., Beutel, T., Lei, G.-D., and Sachtler, W. M. H., *J. Catal.* **158**, 327 (1996).
16. Aylor, A. W., Lobree, L. J., Reimer, J. A., and Bell, A. T., *J. Catal.* **170**, 390 (1997).
17. Ali, A., Alvarez, W. E., Loughran, C. J., and Resasco, D. E., *Appl. Catal. B* **14**, 13 (1997).
18. Lombardo, E. A., Sill, G. A., d'Itri, J. L., and Hall, W. K., *J. Catal.* **173**, 440 (1998).
19. Chang, Y. F., and McCarty, J. G., *J. Catal.* **165**, 1 (1997).
20. Almusaiteer, K., and Chuang, S. S. C., *J. Catal.* **184**, 189 (1999).
21. Konduru, M. K., and Chuang, S. S. C., *J. Phys. Chem. B* **103**, 5802 (1999).
22. London, J. W., and Bell, A. T., *J. Catal.* **31**, 96 (1973).
23. Gandhi, H. S., and Shelef, M., *J. Catal.* **28**, 1 (1973).

24. Hierl, R., Urbach, H.-P., and Knözinger, H., *J. Chem. Soc., Faraday Trans.* **355**, 88 (1992).
25. Dandekar, A., and Vannice, M. A., *J. Catal.* **178**, 621 (1998).
26. Salama, T. M., Ohnishi, R., and Ichikawa, M., *J. Chem. Soc., Faraday Trans.* **92**, 301 (1996).
27. Centi, G., Perthoner, S., Biglino, D., and Giamello, E., *J. Catal.* **151**, 75 (1995).
28. Radtke, F., Koeppel, R. A., Minardi, E., and Baiker, A., *J. Catal.* **167**, 127 (1997).
29. Dekker, F. H. M., Kraneveld, S., Bliek, A., Kapteijn, F., and Moulijn, J. A., *J. Catal.* **170**, 168 (1997).
30. Tanaka, T., Okuhara, T., and Misono, M., *Appl. Catal. B* **4**, L1 (1994).
31. Yasuda, H., Miyamoto, T., and Misono, M., *in* "ACS Symposium Series No. 587, Reduction of Nitrogen Oxide Emission" (U. S. Ozkan, S. K. Agarwal, and G. Marcelin, Eds.), p. 110. Am. Chem. Soc., Washington, DC, 1995.
32. Li, Y., Slager, T. L., and Armor, J. N., *J. Catal.* **150**, 388 (1994).
33. Hayneys, N. W., Joyner, R. W., Shipro, E. S., *Appl. Catal. B* **8**, 343 (1996).
34. Satsuma, A., Enjoji, T., Shimizu, K.-I., Sato, K., Yoshida, H., and Hattori, T., *J. Chem. Soc., Faraday Trans.* **94**, 301 (1998).
35. Caption, D. K., and Amiridis, M. D., *J. Catal.* **184**, 377 (1999).
36. Shimizu, K.-I., Kawabata, H., Satsuma, A., and Hattori, T., *J. Phys. Chem. B* **103**, 5240 (1999).
37. Anderson, J. A., Márquez-Alvarez, C., López-Muñoz, M. J., Rodríguez-Romas, I., and Guerrero-Ruiz, A., *Appl. Catal. B* **14**, 189 (1997).
38. Ukisu, Y., Sato, S., Abe, A., and Yoshida, K., *Appl. Catal. B* **2**, 147 (1993).
39. Long, R. Q., and Yang, R. T., *J. Phys. Chem. B* **103**, 2232 (1999).
40. Li, C., Bethke, K. A., Kung, H. H., and Kung, M. C., *J. Chem. Soc., Chem. Commun.* **8**, 813 (1995).
41. Lobree, L. J., Aylor, A. W., Reimer, J. A., and Bell, A. T., *J. Catal.* **169**, 188 (1997).
42. Chuang, S. S. C., and Tan, C.-D., *J. Catal.* **173**, 95 (1998).
43. Vratny, F., *Appl. Spectrosc.* **13**, 59 (1959).
44. Addison, C. C., and Gatehouse, B. M., *J. Chem. Soc.* 613 (1960).
45. Ferraro, J. R., *J. Mol. Spectrosc.* **99**, 4 (1960).
46. Xie, Y.-C., and Tang, Y.-Q., *Adv. Catal.* **37**, 1 (1990).
47. Nakamoto, K., "Infrared and Raman Spectra of Inorganic and Coordination Compounds," 4th ed. Wiley, New York, 1986.
48. Davydov, A. A., *in* "Infrared Spectra of Adsorbed Species on the Surface of Transition Metal Oxides" (C. H. Rochester, Ed.), Wiley, England, 1990.
49. Laane, J., and Ohlsen, J. R., *Prog. Inorg. Chem.* **27**, 465 (1980).
50. Outka, D. A., and Madix, R. J., *Surf. Sci.* **179**, 1 (1987).
51. Hadjiivanov, K., Klissurski, D., Ramis, G., and Busca, G., *Appl. Catal. B* **7**, 251 (1996).
52. Delahay, G., Coq, B., Ensuque, E., and Figuéras, F., *Langmuir* **13**, 5588 (1997).
53. Trout, B. L., Chakraborty, A. K., and Bell, A. T., *J. Phys. Chem.* **100**, 17582 (1996).
54. Colthup, N. B., Daly, L. H., and Wiberley, S. E., "Introduction to Infrared and Raman Spectroscopy," 3rd ed. Academic Press, San Diego, 1990.
55. Silverstein, R. M., and Webster, F. X., "Spectrometric Identification of Organic Compounds," 6th ed. Wiley, England, 1997.
56. Escribano, V. S., Busca, G., and Lorenzelli, V., *J. Phys. Chem.* **94**, 8939 (1990).
57. Kiss, J., and Solymosi, F., *J. Catal.* **179**, 277 (1998).
58. Morterra, C., Magnacca, G., and Favero, N. D., *Langmuir* **9**, 642 (1993).
59. Chi, Y., Preliminary research of Ph.D. thesis, The University of Akron, 1999.
60. Levenspiel, O., "Chemical Reaction Engineering," 3rd ed., p. 55. Wiley, New York, 1999.
61. Djonev, B., Tsyntsarski, B., Klissurski, D., and Hadjiivanov, K., *J. Chem. Soc., Faraday Trans.* **93**, 4055 (1997).
62. Okuhara, T., Hasada, Y., and Misono, M., *Catal. Today* **35**, 83 (1997).